Ion energy distribution measurements in rf and pulsed dc plasma discharges

Gahan, D.; Hayden, C.; Scullin, P.; O'Sullivan, D.; Pei, Yutao T.; Hopkins, M. B.; O'Sullivan, D.; Daniels, S.

Published in:
Plasma sources science & technology

DOI:
10.1088/0963-0252/21/2/024004

Publication date:
2012

Plasma Sources Sci. Technol. **21** (2012) 024004 (8pp) doi:10.1088/0963-0252/21/2/024004

Ion energy distribution measurements in rf and pulsed dc plasma discharges

D Gahan[1], S Daniels[2], C Hayden[2], P Scullin[1], D O'Sullivan[1], Y T Pei[3] and M B Hopkins[1]

[1] Plasma Research Group, Impedans Ltd., Unit 8 Woodford Court, Woodford Business Park, Santry, Dublin 17, Ireland
[2] National Centre for Plasma Science and Technology, Dublin City University, Dublin 9, Ireland
[3] Department of Applied Physics, Materials innovation institute M2i, University of Groningen, Nijenborgh 4, 9747 AG Groningen, The Netherlands

E-mail: david.gahan@impedans.com

Received 2 August 2011, in final form 7 December 2011
Published 4 April 2012
Online at stacks.iop.org/PSST/21/024004

Abstract
A commercial retarding field analyzer is used to measure the time-averaged ion energy distributions of impacting ions at the powered electrode in a 13.56 MHz driven, capacitively coupled, parallel plate discharge operated at low pressure. The study is carried out in argon discharges at 10 mTorr where the sheaths are assumed to be collisionless. The analyzer is mounted flush with the powered electrode surface where the impacting ion and electron energy distributions are measured for a range of discharge powers. A circuit model of the discharge, in combination with analytical solutions for the ion energy distribution in radio-frequency sheaths, is used to calculate other important plasma parameters from the measured energy distributions. Radio-frequency compensated Langmuir probe measurements provide a comparison with the retarding field analyzer data. The time-resolved capability of the retarding field analyzer is also demonstrated in a separate pulsed dc magnetron reactor. The analyzer is mounted on the floating substrate holder and ion energy distributions of the impinging ions on a growing film, with 100 ns time resolution, are measured through a pulse period of applied magnetron power, which are crucial for the control of the microstructure and properties of the deposited films.

(Some figures may appear in colour only in the online journal)

1. Introduction

Plasma processes are used extensively in modern industry for surface modification. Substrates exposed to the plasma are bombarded by energetic ions including reactive species. The energy and flux of bombarding ions play an important role in the removal (etching) and deposition of layers on the substrate surface. Asymmetric radio-frequency (rf) capacitively coupled plasma (CCP) reactors are commonly used for plasma etching. The rf excitation voltage applied to the powered electrode (which hosts the substrate) controls the flux and energy of the bombarding ions. Pulsed magnetron sputtering reactors are often used for depositing thin films. The target is driven with a pulsed dc (p-dc) bias to excite the plasma and sputter the target atoms. Monitoring of the flux and energy of ions arriving at the substrate in these reactors is now essential for process optimization and the control of films microstructure.

Commercial plasma reactors, such as the Oxford Instruments Plasmalab System 100 [1] reactive ion etcher (RIE) and the TEER UDP400/4 closed-field unbalanced magnetron sputtering system used in this study, are rarely equipped with plasma diagnostics. Electrical probes (Langmuir probes, etc) that require insertion into the discharge are often not practical in processing reactors for many reasons—contamination and plasma perturbation being the most important. Voltage–current (*VI*) probes mounted on the power feed line have been shown to be a powerful non-invasive diagnostic [2–7]. They provide the user with a direct measurement of the excitation voltage and plasma current waveforms. These waveforms can be used to calculate

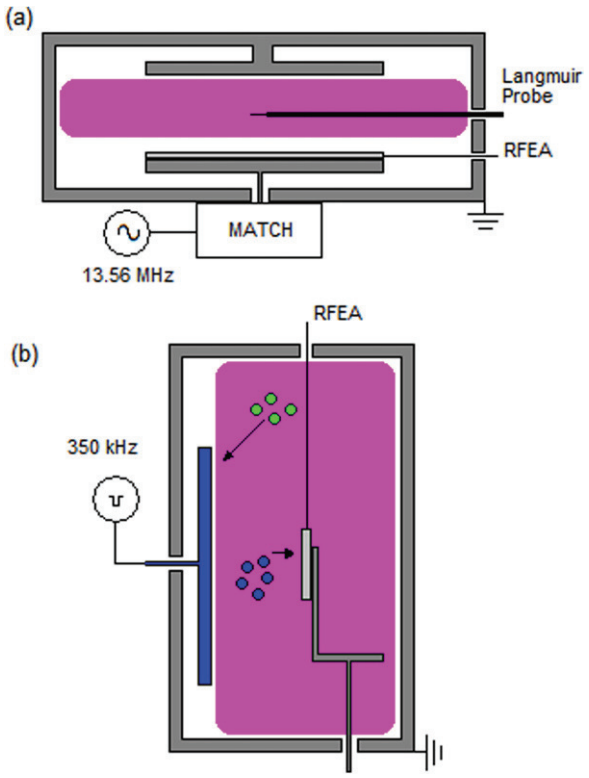

Figure 1. (*a*) Schematic of the CCP reactor showing the location of the RFEA and Langmuir probe. (*b*) Schematic of the magnetron sputtering reactor showing the pulsed biased target and the location of the RFEA. The argon ions (green dots) from the discharge sputter the titanium atoms (blue dots) from the target which in turn become deposited on the substrate.

important plasma parameters such as ion flux and ion energy in rf discharges [8, 9].

In this work, the ion energy distribution functions (IEDFs) and ion fluxes have been measured directly with a commercial retarding field energy analyzer (RFEA), Semion^{TM} System 500 [10]. In the CCP reactor the RFEA is located at the powered electrode (see figure 1(*a*)) while in the magnetron reactor it is attached to the substrate holder (figure 1(*b*)). In this way the RFEA is minimally invasive.

RFEAs have been used for decades to measure IEDFs in plasma discharges. Some designs require that they be mounted on a grounded surface [11–17] to avoid complications with biasing. Electrically filtered RFEAs [18–20] and optically isolated floating RFEAs [21–25] have also been developed, enabling direct measurement of the IEDF at biased surfaces. Mechanical miniaturization of RFEA designs has removed the need for differential pumping, at low pressures, when the dimensions are less than the ion mean free path. The commercial analyzer used here incorporates the miniature design to avoid differential pumping and uses high impedance low-pass filters to allow the RFEA to float at the electrode bias potential for frequencies in the range of 1 kHz to 100 MHz. High-temperature cabling connects the analyzer to the data acquisition unit through a vacuum feed-through at the reactor wall.

This paper focuses on time-averaged RFEA measurements in an argon rf CCP discharge at 10 mTorr. The time-resolved capabilities of the RFEA are also demonstrated in a p-dc magnetron discharge with argon sputtering gas and a titanium target at 2 mTorr. In section 2 the experimental setups are described. In section 3 a simple circuit model of the rf CCP discharge, similar to that used by Kohler *et al* [26, 27], is introduced and a number of analytical models of the IEDF in rf sheaths [28–30] are summarized. These models are combined with the measured IEDFs in the CCP reactor to estimate other important plasma parameters. In section 4 IEDF and electron energy distribution (EEDF) measurements, as a function of argon discharge power, are presented for the CCP reactor. Parameters obtained from the IEDF measurements are used to solve the discharge circuit model and the analytical IEDF models. A method for determining the ion flux to the electrode is presented, which is independent of the ion current detected by the RFEA. The time-resolved IEDF measurements at the substrate holder in the magnetron reactor are also presented in section 4. Finally, in section 5 the main conclusions of this study are summarized.

2. Experimental

2.1. CCP plasma reactor

The commercial CCP reactor is a Plasmalab System 100 parallel plate RIE plasma tool with 200 mm diameter electrodes. The working gas is supplied through a shower head configuration in the grounded electrode. The gap between the two electrodes is approximately 4.5 cm. There is no radial confinement of the plasma—it extends to the earthed reactor walls. The earthed area, in contact with the plasma, is therefore much larger than the powered electrode area. This type of discharge has become known as an asymmetric CCP. Power is coupled to the lower electrode, through a blocking capacitor in the matching unit, in the range 10–100 W at a single frequency of 13.56 MHz. Figure 1(*a*) gives a schematic of the reactor showing the location of the RFEA and the Langmuir probe. The Langmuir probe tip is centered above the sampling orifices of the RFEA in the mid-plane of the discharge gap. The RFEA is mounted directly on the powered electrode.

2.2. Magnetron sputtering reactor

The magnetron sputtering reactor used is a TEER UDP400/4 closed-field unbalanced magnetron sputtering system. More details on this experimental setup can be found in [31]. A p-dc current at 350 kHz was applied to one titanium target $200 \times 100\,\text{mm}^2$ to create a discharge in the argon working gas at approximately 2 mTorr. The RFEA was attached to the substrate holder and oriented in such a way that the orifice was directly facing the biased target. The experimental setup is sketched in figure 1(*b*).

2.3. Retarding field energy analyzer

A sketch of the commercial RFEA (Semion^{TM} system) is sketched in figure 2(*a*). Ions enter the RFEA through a sampling aperture exposed to the plasma. A grid parallel to the orifice plate is biased with a potential sweep to create a

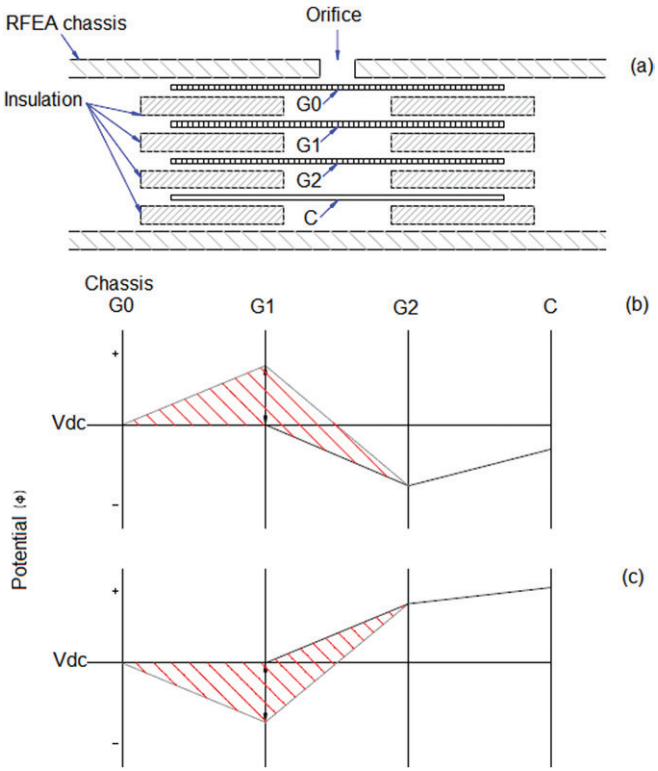

Figure 2. (*a*) Schematic of the RFEA construction, (*b*) RFEA potential configuration for ion discrimination, (*c*) RFEA potential configuration for electron discrimination.

potential barrier for the charged plasma species of interest. A detector plate parallel to the grid collects the current of charged particles with sufficient energy to overcome the potential barrier at each point in the bias sweep. The IEDF is determined by differentiating the resultant current–voltage characteristic. The operation of this device has been discussed extensively in previous publications [20, 32–33]. Ions are sampled through an orifice which faces the plasma. The RFEA is 70 mm in diameter and 5 mm thick and made from aluminum. It is mounted on the powered electrode as described in the previous section (see figure 1(*a*)). Only one orifice is sketched, for clarity, but in reality there is an array of 800 μm diameter orifices, with a sampling area of approximately 20 mm^2, which maintains a measurable ion flux through the analyzer.

The first grid, G_0, covers the orifice array and has an aperture size of 25 μm. This grid ensures that the diameter of the open area, 'seen' by the plasma, is less than the Debye length and prevents plasma extending inside the device. A second grid, G_1, is biased with either a negative or positive potential sweep (with respect to the dc potential of G_0 the chassis) to discriminate plasma electrons or ions, respectively, in terms of their energy. A third grid, G_2, is biased with a fixed negative or positive potential to repel the unwanted charged species from the detector.

Configuring the device such that G_2 repels the unwanted charged species has the added advantage that it also prevents secondary electron emission from the detector plate which would otherwise result in an erroneous contribution to the current–voltage characteristic. The collector plate is always biased negatively to attract the ions for detection. The potential configurations for ion and electron energy discrimination are sketched in figures 2(*b*) and (*c*), respectively.

The analyzer (including G_0, G_1, G_2 and C) is enabled to float at the ac component of the applied bias signal. This is achieved by means of high impedance low-pass filters. These high impedance filters prevent short circuiting of the applied bias signal to ground and provide sufficient attenuation at the output to protect the measurement electronics. The RFEA chassis also floats at the dc component of the applied bias signal. The required dc electric fields between adjacent grids are produced by setting the grid potentials relative to the dc component $\bar{V}_{dc}$ of the applied bias. The analyzer incorporates a direct measurement of $\bar{V}_{dc}$, allowing the user to compensate for dc bias at the sensor chassis. At each step in the discriminating potential sweep only ions with sufficient energy to overcome the potential barrier reach the collector plate for detection. The resultant discriminator potential versus collector current characteristic is differentiated to give the IEDF. The acceptance angle of a sampling orifice is approximately 45° allowing detection of ions arriving at the surface within this angle. The measured IEDF is the energy distribution of the ions perpendicular to the electrode surface.

3. Theoretical modeling

3.1. CCP circuit model

A simple circuit model of an asymmetric rf CCP discharge has been derived by Kohler *et al* [27]. This model is used here to obtain an expression for the rf component of the powered sheath potential. This expression for the powered rf sheath potential is used to solve the analytical IEDF models described in section 3.2.

The model assumes that the rf potential $V_{rf}(t)$ at the electrode has the form $V_{rf}(t) = \bar{V}_{dc} + \tilde{V}_{rf} \sin \omega t$, where $\bar{V}_{dc}$ is the self-bias voltage developed on the blocking capacitor and $\tilde{V}_{rf}$ is the amplitude of the rf component of the excitation voltage. This model does not incorporate harmonic components of the driving voltage that may be induced by the nonlinear sheath impedance. The grounded area in contact with the plasma is much larger than the powered electrode area since the unconfined plasma is in contact with both the grounded electrode and the reactor walls. The result is that the driven sheath is much thicker than the ground sheath. Figure 3(*a*) shows the equivalent circuit proposed by Kohler *et al* [27]. If the capacitive sheath approximation is assumed then the resistive components are negligible, i.e. R_{ps} and $R_{ws} \to \infty$, $R_p \to 0$. If the sheaths are approximated as pure capacitances then a fraction of the powered electrode potential is dropped across the ground sheath and the plasma potential will have the form $V_p(t) = \bar{V}_p + \tilde{V}_p \sin \omega t$, where $\bar{V}_p$ is the time-averaged plasma potential and $\tilde{V}_p$ is the amplitude of the rf component of the plasma potential. $\tilde{V}_p$ is determined by capacitive voltage division, of the rf component of the excitation potential, between the time-averaged powered and ground sheath capacitances. The ratio of the sheath capacitances is dependent on the relative areas in contact with the discharge and on the discharge parameters.

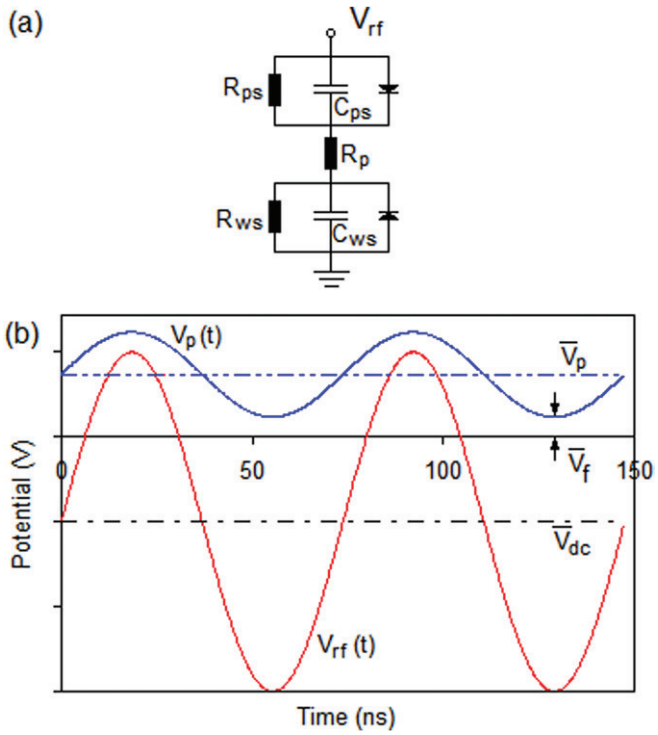

Figure 3. (*a*) Equivalent circuit of asymmetric rf CCP where R_{ps} and C_{ps} are the powered sheath resistance and capacitance, respectively, and R_{ws} and C_{ws} are the wall/ground sheath resistance and capacitance, respectively. R_p is the bulk plasma resistance. (*b*) Illustrative discharge potentials where $V_{rf}(t)$ and $\bar{V}_{dc}$ are the excitation potential and dc self-bias, respectively, and $V_p(t)$ and $\bar{V}_p$ are the time-varying and time-averaged components of the plasma potential, respectively. $\bar{V}_f$ is the plasma floating potential.

Figure 3(*b*) shows a sketch of the powered electrode potential and the plasma potential based on this model. The result of capacitive coupling is that there can be no net current through the discharge. The electrode potential must approach the plasma potential for a brief period of the rf cycle to allow the electron current to balance the ion flux. Similarly, the plasma potential must also approach the ground potential for the same reason. The plasma potential never quite reaches the powered electrode potential or ground potential—the minimum potential difference between the two can be more accurately approximated as the plasma floating potential $\bar{V}_f$. However, it can be assumed in this case that $\bar{V}_f \ll \bar{V}_{dc}$ and the well-known expression for the time-averaged plasma potential $\bar{V}_p$ is given by

$$\bar{V}_p = \tfrac{1}{2}(\tilde{V}_{rf} + \bar{V}_{dc}). \tag{1}$$

The energy of the ions reaching the powered electrode is controlled by the magnitude of the rf voltage drop across the adjacent sheath. The amplitude of the sheath voltage $\tilde{V}_s$ is defined as

$$\tilde{V}_s = \tilde{V}_{rf} - \tilde{V}_p. \tag{2}$$

The amplitude of the rf sheath potential can then be written in terms of the time-averaged plasma potential and the electrode dc bias voltage

$$\tilde{V}_s = \bar{V}_p - \bar{V}_{dc}. \tag{3}$$

This is particularly convenient since the time-averaged plasma potential and dc bias voltage can be measured directly with the RFEA.

3.2. Theoretical ion energy distributions

The IEDF generated by an oscillating, collisionless rf sheath has been solved analytically by a number of authors [28–30]. The shape of the ion energy distribution in a collisionless rf plasma sheaths is determined by the ratio of the ion transit time to the period of the rf cycle τ_i/τ_{rf}. The ion transit time is the length of time taken for an ion to traverse the sheath when the sheath is at its mean (dc) value $\bar{V}_s$. These analytical models assume that the mean sheath width $\bar{s}$ can be written in terms of $\bar{V}_s$ using the well-known Child–Langmuir law [34, 35]

$$\bar{s} = \frac{2}{3}\left(\frac{2e}{M_i}\right)^{1/4}\left(\frac{\varepsilon_0}{\bar{J}_i}\right)^{1/2}\bar{V}_s^{3/4}, \tag{4}$$

where e is the electronic charge, M_i is the ion mass, ε_0 is vacuum permittivity and $\bar{J}_i$ is the ion current density in the sheath. The ion transit time is then written as follows [36]:

$$\tau_i = 3\bar{s}\left(\frac{M_i}{2e\bar{V}_s}\right)^{\frac{1}{2}}. \tag{5}$$

When a sinusoidal potential is applied to the sheath the calculated IEDF is the standard bi-modal (saddle-shaped) structure with peak separation controlled by the ratio τ_i/τ_{rf}. In the situation where $\tau_i/\tau_{rf} \ll 1$, the ions cross the sheath in a small fraction of the rf cycle and the peak separation ΔE is approximately equivalent to the peak-to-peak sheath voltage $V_{pp} = 2\tilde{V}_s$ such that $\Delta E \approx eV_{pp}$. The midpoint between the two peaks in the bi-modal energy distributions $e\bar{V}_s$ is equivalent to the time-averaged sheath potential, i.e. it corresponds to the energy an ion gains when accelerated through the time-averaged sheath potential $\bar{V}_s$.

For CCP sheaths driven at 13.56 MHz the ions may take many rf cycles to cross, i.e. $\tau_i/\tau_{rf} \gg 1$. The peak separation narrows considerably, relative to eV_{pp}, and becomes single peaked when τ_i/τ_{rf} is sufficiently large. The ΔE for IEDFs created in this regime has been calculated by Benoit-Caittin *et al* [28] assuming a collisionless rf sheath and a sinusoidal sheath potential waveform

$$\Delta E = \frac{2eV_{pp}}{\pi}\left(\frac{\tau_{rf}}{\tau_i}\right). \tag{6}$$

Charles *et al* [30] find a similar expression using a simple fit to a series of ΔE values calculated using a self-consistent fluid model of the plasma sheath, across the entire range of possible values for τ_i/τ_{rf}. The result of Charles *et al* [30], expressed in terms of the variables used in this paper, is

$$\Delta E = eV_{pp}\left(1 + \left(\frac{2\pi\tau_i}{3\tau_{rf}}\right)^2\right)^{-1/2}. \tag{7}$$

An analytical expression for ΔE for all values of τ_i/τ_{rf} is also given by Sobolewski *et al* [29] which uses the rf sheath

model described in [37]. This model is solved in terms of the ion plasma frequency at the sheath edge rather than the ion transit time. When the ion plasma frequency is much less than the rf bias frequency the ions do not respond to the full rf sheath voltage. The model calculates an effective rf sheath potential which is a damped version of the true rf sheath potential and represents the actual potential 'seen' by the ions. The characteristic frequency of the damping is the ion plasma frequency ω_{i}. For consistency with other models Soblewski *et al* [29] have also derived their expression in terms of τ_{i}. The result of [29], expressed in terms of the variables defined in this paper, is

$$\Delta E = eV_{\mathrm{pp}}\left(1+\pi^2\left(\frac{2kT_{\mathrm{e}}}{\bar{V}_{\mathrm{s}}}\right)^{1/2}\left(\frac{\tau_{\mathrm{i}}}{\tau_{\mathrm{rf}}}\right)^2\right)^{-1/2}, \qquad (8)$$

where kT_{e} is the electron temperature.

Equations (7) and (8) have been re-derived in terms of the ion transit time given by equation (5), for consistency, since the original authors use slightly different expressions for the ion transit time.

4. Results and discussion

4.1. Measured energy distributions in the CCP reactor

Time-averaged IEDFs at the powered electrode and EEDFs in the bulk plasma have been measured in argon discharges at 10 mTorr at discharge powers in the range 10–100 W where the sheaths can be assumed to be collisionless. Figure 4(*a*) shows the measured IEDFs as a function of discharge power. The main feature of the IEDF is the bi-modal, saddle-shaped structure—the height and separation of the two peaks increasing with increasing power.

The height of the peaks, or more accurately the area under the IEDF, is proportional to the ion flux to the electrode. From equations (6)–(8) it can seen that the peak separation is approximately proportional to the rf bias voltage; however, the 'constant' of proportionality τ_{i} is itself weakly dependent on voltage. In these experiments both ion flux and rf bias voltage increase with increasing rf power. The rf sheath potential and the analytical IEDF models are solved using parameters determined directly from the measured IEDFs, i.e. ΔE, $e\bar{V}_{\mathrm{s}}$ and $\bar{V}_{\mathrm{dc}}$.

In figure 4(*b*) the Langmuir probe EEDF measurements in the bulk plasma as a function of discharge power are shown. The EEDFs are bi-Maxwellian with the two temperatures remaining approximately constant as a function of power. The bi-Maxwellian EEDF is now a well understood feature of low pressure CCP discharges [38].

4.2. Ion flux to the electrode

There are a number of ways to determine the ion flux to the powered electrode using the current setup. Using the Langmuir probe measurements of electron temperature and ion density in the bulk plasma the ion flux is estimated from

$$\bar{J}_{\mathrm{i}} = 0.6en_{\mathrm{e}}\sqrt{\frac{kT_{\mathrm{e}}}{m_{\mathrm{i}}}}, \qquad (9)$$

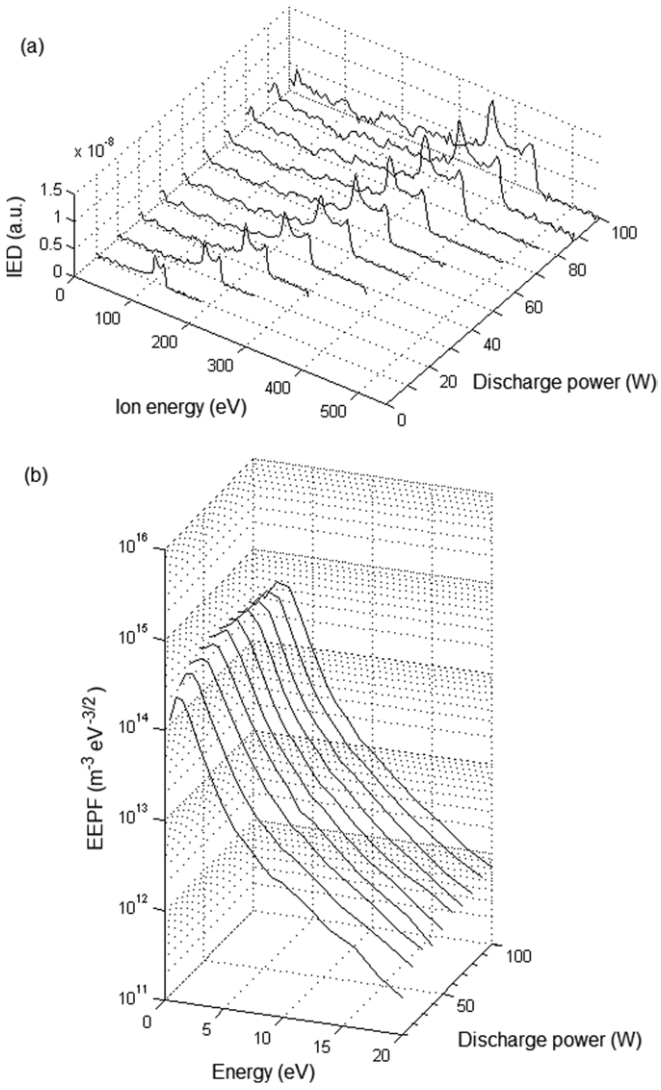

Figure 4. (*a*) Ion energy distributions versus rf power and (*b*) EEDF versus rf power in the bulk plasma. All measurements are made in argon discharges at 10 mTorr.

where $(kT_{\mathrm{e}}/m_{\mathrm{i}})^{1/2}$ is the Bohm velocity and n_{e} is the electron density. The factor of 0.6 is used to account for the plasma density drop between the mid-plane of the bulk plasma (where the Langmuir probe is situated) and the sheath edge. Equation (9) applies for a Maxwellian EEDF. It has been shown [39] that for a bi-Maxwellian EEDF the Bohm velocity is largely determined by the low-temperature electron population. Equation (9) is solved using the low electron temperature values calculated from the EEDFs presented in figure 4(*b*).

The ion flux is also estimated from the total ion current detected by the RFEA. The orifice sampling area and the transmission of the three grids must be accounted for such that

$$\bar{J}_{\mathrm{i}} = \frac{I_{\mathrm{C}}}{TA}, \qquad (10)$$

where I_{C} is the total ion current reaching the collector, T is the effective transmission of the three layers of grids and A is the sampling orifice area. Other effects may result in this

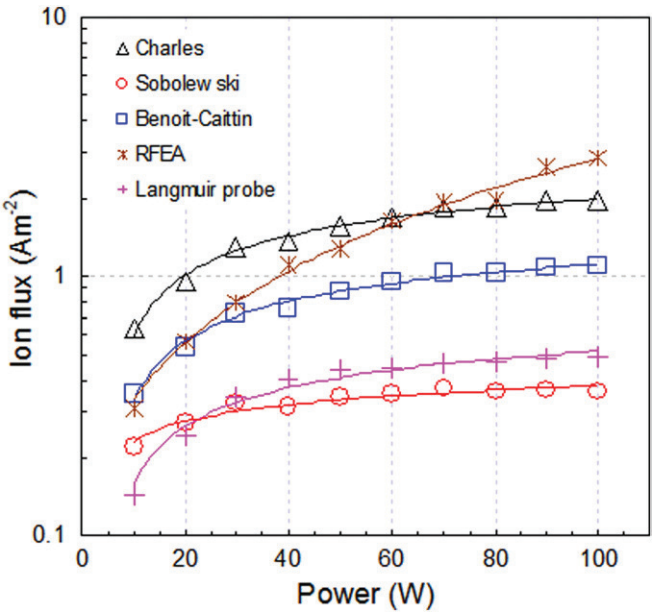

Figure 5. Ion flux as a function of discharge power determined from the five methods described in the text.

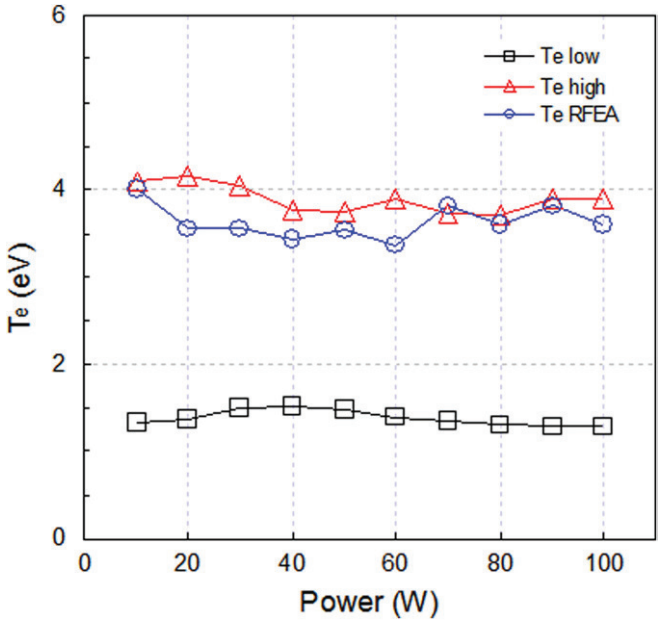

Figure 6. Comparison of the electron temperature determined with the RFEA to the electron temperature determined with the Langmuir probe.

equation being inaccurate under certain plasma conditions. Ion scattering due to elastic ion–neutral collisions must be considered, especially at elevated pressures where the ion mean free path becomes comparable to the analyzer dimension. Secondary electron emission from surfaces within the RFEA, ion dispersion and grid misalignment are factors that should also be considered [25].

Another method, independent of the measured RFEA current, based on the measured IEDF can also be used to estimate the ion flux. Inserting (4) into (5) and solving for the ion flux gives the following expression:

$$\bar{J}_\mathrm{i} = \frac{\varepsilon_0}{\tau_\mathrm{i}^2}\sqrt{\frac{8m_\mathrm{i}\bar{V}_\mathrm{s}}{e}}. \tag{11}$$

The ion transit time is determined from the three analytical IEDF models defined by equations (6), (7) and (8) using ΔE from the measured IEDFs and V_pp calculated from equation (3). The results of the ion flux calculations from (9), (10) and (11) are shown in figure 5. The shapes of the curves obtained from the Langmuir probe, the Charles *et al* model and the Benoit-Cattin *et al* model, are in excellent qualitative agreement. The Langmuir probe measurements are consistently lower, but it is known that Langmuir probes can underestimate the electron density since they can deplete the plasma in the vicinity of the probe. This, combined with the many simplifying assumptions inherent in the discharge circuit model can account for the quantitative disagreement. By incorporating a direct measurement of rf bias voltage, and possibly a more sophisticated discharge circuit model, better quantitative agreement should be obtained. The ion flux determined directly from the RFEA current and that determined using Sobolewski *et al* scale differently from the other methods. Equation (8) is the general solution of Sobolewski's expression and as such contains extra variables when compared with equations (6) and (7), i.e. the ratio of kT_e to $\bar{V}_\mathrm{s}$. To solve this equation the Langmuir probe measurements of kT_e must be used. The error associated with measuring kT_e may be a contributing factor to the discrepancy with the other models. The ion flux calculated from the RFEA diverges from the other methods at discharge powers above 30 W. This indicates that the effective transmission of the grid layers is energy dependent.

4.3. Electron temperature and EEDF

The electron temperature, or more importantly the EEDF, is an important plasma parameter which determines properties such as ion flux to the surface and controls chemical reactions in the discharge. In this section the EEDF measurements determined with a Langmuir probe are compared with those determined with the RFEA.

The EEDF is measured with the RFEA in a similar way to the IEDF, except that the polarity of the biases applied to the various grids are reversed. The logarithm of the electron current, for all experiments conducted, was linear with energy—indicating a Maxwellian EEDF. However, the EEDFs measured with the Langmuir probe in the bulk plasma are bi-Maxwellian. Figure 6 shows the electron temperatures determined from the high- and low-energy populations of the Langmuir bi-Maxwellian EEDF and the temperature of the RFEA Maxwellian EEDF. The electron temperature from the RFEA is in excellent agreement with the high electron temperature from the Langmuir probe. There is no conflict between the RFEA and Langmuir probe EEDF measurements. The Langmuir probe located in the bulk plasma is biased from an external source and is therefore able to sample the entire EEDF. The RFEA is attached to the powered electrode and can only detect electrons that have sufficient energy to cross

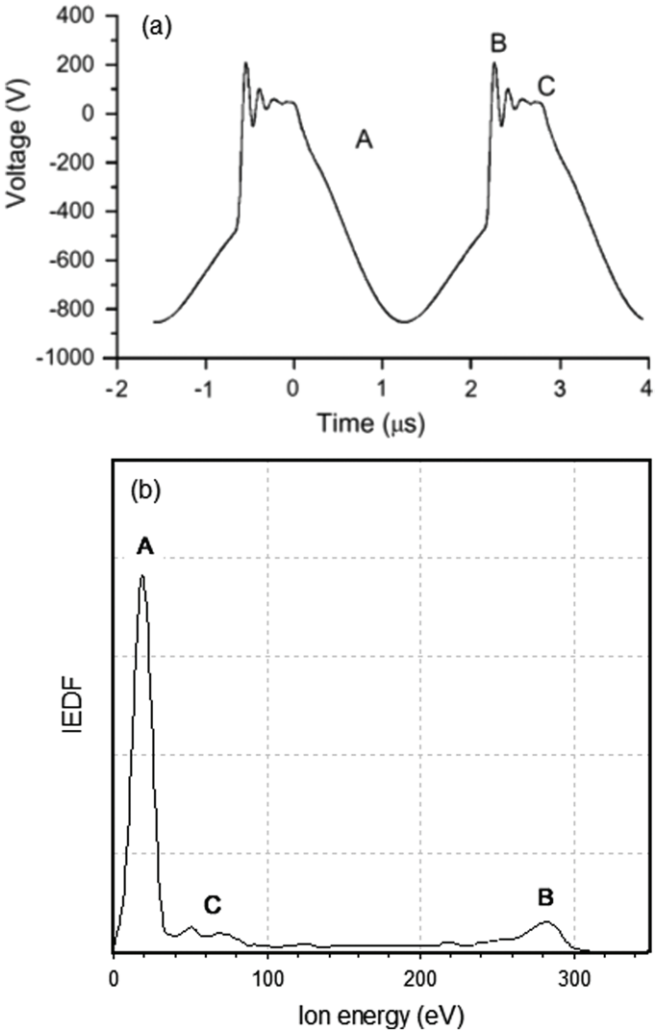

Figure 7. (*a*) Bias waveform applied to the target in a magnetron sputtering reactor and (*b*) time-averaged ion energy distribution measured at the substrate holder, where the IEDF axis has a linear scaling.

the minimum potential of the adjacent sheath. It is expected that the minimum potential difference between plasma and electrode is the floating potential (see figure 3) which is approximately constant at +20 V throughout. Therefore, the RFEA can only detect the high-energy tail of the EEDF. This is corroborated by the excellent agreement between RFEA electron temperatures and the high electron temperature from the Langmuir probe.

4.4. Time-resolved IEDF in a pulsed magnetron reactor

Figure 1(*b*) shows a schematic of the experimental setup used to demonstrate the time-resolved capability of this RFEA. A typical p-dc bias waveform applied to the titanium target is shown in figure 7(*a*). This reactor is used for sputtering layers of the target material onto various substrates. The RFEA is mounted on the substrate holder facing the target. The target bias frequency is set to 350 kHz while the substrate holder is electrically floating. Three distinct phases, labeled A, B and C, associated with the 'on' time, a 'ringing' period

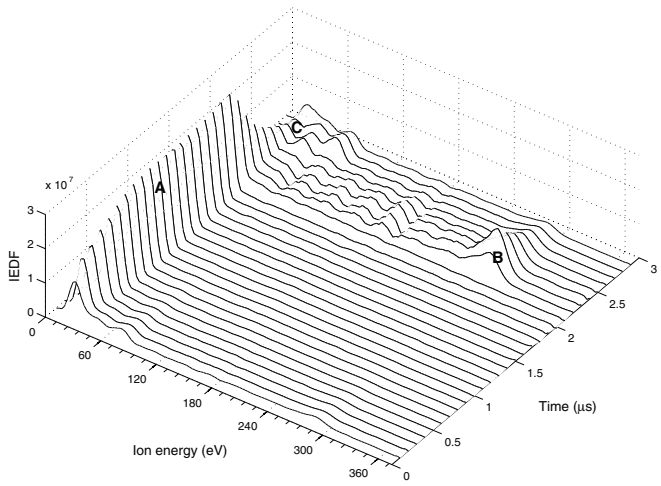

Figure 8. Time resolved ion energy distributions with 100 ns time resolution through the p-dc cycle.

and an 'off' time, respectively, can be identified [31]. The time-averaged IEDF at the substrate position is shown in figure 7(*b*). A number of ion energy peaks are visible. It can be difficult to determine at which time in the p-dc cycle the various energy peaks are created from the time-averaged measurement. Therefore the IEDF has been measured with 100 ns time resolution during the pulse period, as shown in figure 8. The energy peaks associated with phases A, B and C of the bias waveform are highlighted.

During phase A the large negative potential that excites the discharge is applied. The plasma forms and stabilizes at a relatively low positive potential. This potential accelerates ions to the floating substrate. The energy of the ions during this phase of the bias period is approximately 20 eV.

When the pulse is switched off the potential drops toward zero and actually overshoots to a large positive value. This overshoot is induced by interactions between the power supply and the discharge. The positive overshoot forces the plasma to a large positive potential during this phase of the bias period. The ions are now accelerated to the substrate with much higher energy. Figure 8 shows that the ion energy during period B increases to approximately 300 eV in this case.

There is also a pulse-off period (sometimes called the reverse period) which is set to 500 ns in this experiment. During this period the target potential settles to a relatively small positive potential. Again, the plasma potential must be the most positive potential in the system and settles to a more positive value than during the on time. The result is that ions are accelerated to a slightly higher energy during this phase of the bias period. From figures 7 and 8 we see that the ion energy during this period is approximately 50 eV.

Such a wide energy distribution of impinging ions is essential for obtaining ultra-smooth films according to the atomistic impact-induced downhill flow model [40] and the experimental validation [41]. Accordingly, the time-resolved IEDF with a nanosecond time resolution provides critical information for the design of pulse waveform in p-dc power sources in terms of IED optimization for the control of films microstructure and properties.

5. Conclusion

An RFEA located at the powered electrode of an asymmetric rf CCP discharge is used to measure time-averaged ion energy distributions behind the powered sheath at 10 mTorr argon pressure. Under these conditions the IEDF has the recognizable bi-modal, saddle-shaped structure and the sheath can be assumed collisionless.

A number of methods were used to determine the ion flux to the electrode. Good qualitative agreement was obtained between Langmuir probe measurements and the solution of equation (11) using the theoretical IEDF models derived by Charles *et al* and Benoit-Cattin *et al*. The method based on equation (11) is independent of the RFEA current, which can be difficult to interpret, and has the potential to be used as a method for calibrating RFEAs for absolute ion flux. It was found that the RFEA collector current did not scale as expected indicating that the RFEA collector current is a function of both ion flux and ion energy, for the RFEA used in this study.

The EEDF reaching the electrode has also been measured and compared with the EEDF in the bulk plasma. It has been shown that the bulk EEDF is bi-Maxwellian, as expected for low-pressure rf CCPs. Only the high-temperature electron population has sufficient energy to reach the electrode for detection with the RFEA. The temperature of the EEDF measured with the RFEA is in excellent agreement with the temperature of the high-energy electron population measured with the Langmuir probe.

In p-dc discharges the bias frequency is considerably lower, 350 kHz in this case. The complex bias waveforms employed tend to cause dramatically different impact ion energies during different phases of the bias period. It is important therefore to measure both time-averaged and time-resolved ion energies. The nature of the RFEA generally makes it difficult to achieve good time resolution. The RFEA used in this study incorporates a novel filter design that enables 100 ns time resolution. The capabilities of this design are demonstrated in a pulsed magnetron discharge. The 100 ns time steps clearly show the transitions between phases of the bias waveforms through the ion energy distribution measurements.

Acknowledgment

Parts of this work were supported by Science Foundation Ireland (SFI) under grant number 08/SRC/I1411.

References

[1] www.oxford-instruments.com
[2] Sobolewski M A 1992 *J. Vac. Sci. Technol.* A **10** 3550
[3] Sobolewski M A 1995 *IEEE Trans. Plasma. Sci.* **23** 6
[4] Godyak V A, Piejak R B and Alexandrovich B M 1991 *IEEE Trans. Plasma. Sci.* **19** 4
[5] Spiliopoulos N, Mataras D and Rapakoulias D E 1996 *J. Vac. Sci. Technol.* A **14** 2757
[6] Mahony C M O, Maguire P D and Graham W G 2005 *Plasma Sources Sci. Technol.* **14** S60
[7] Godyak V A, Piejak R B and Alexandrovich B M 1999 *J. Appl. Phys.* **85** 703
[8] Sobolewski M A 1998 *Appl. Phys. Lett.* **72** 1146
[9] Sobolewski M A 2006 *J. Vac. Sci. Technol.* A **24** 1892
[10] www.impedans.com
[11] Ingram S G and Braithwaite N St J 1988 *J. Phys. D: Appl. Phys.* **21** 1496
[12] Ingram S G and Braithwaite N St J 1990 *J. Appl. Phys.* **68** 5519
[13] Bohm C and Perrin J 1993 *Rev. Sci. Instrum.* **64** 31
[14] Charles C, Boswell R W and Porteous R K 1992 *J. Vac. Sci. Technol.* A **10** 398
[15] Charles C 1993 *J. Vac. Sci. Technol.* A **11** 157
[16] Wild C and Koidl P 1989 *Appl. Phys. Lett.* **54** 505
[17] Wild C and Koidl P 1991 *J. Appl. Phys.* **69** 2909
[18] Woodworth J R, Riley M E, Meister D C, Aragon B P, Le M S and Sawin H H 1996 *J. Appl. Phys.* **80** 1304
[19] Woodworth J R, Abraham I C, Riley M E, Miller P A, Hamilton T W, Aragon B P, Shul R J and Willison C G 2002 *J. Vac. Sci. Technol.* A **20** 873
[20] Gahan D, Dolinaj B and Hopkins M B 2008 *Rev. Sci. Instrum.* **79** 033502
[21] Kuypers A D and Hopman H J 1990 *J. Appl. Phys.* **67** 1229
[22] Kuypers A D and Hopman H J 1988 *J. Appl. Phys.* **63** 1894
[23] Edelberg E A, Perry A J, Benjamin N and Aydil E S 1999 *Rev. Sci. Instrum.* **70** 2689
[24] Manenschijn A, Janssen G C A M, Van der Drift E and Radelaar S 1991 *J. Appl. Phys.* **69** 1253
[25] Baloniak T, Reuter R, Flotgen C and Von Keudell A 2010 *J. Phys. D: Appl. Phys.* **43** 055203
[26] Koenig H R and Maissel L I 1970 *IBM J. Res. Dev.* **14** 168
[27] Kohler K, Coburn J W, Horne D E, Kay E and Keller J H 1985 *J. Appl. Phys.* **57** 59
[28] Benoit-Cattin P and Bernard L C 1968 *J. Appl. Phys.* **39** 5273
[29] Sobolewski M A, Wang Y and Goyette A 2002 *J. Appl. Phys.* **91** 10
[30] Charles C, Degeling A W, Sheridan T E, Harris J H, Lieberman M A and Boswell R W 2000 *Phys. Plasmas* **7** 12
[31] Pei Y T, Chen C Q, Shaha K P, De Hosson J Th M, Bradley J W, Voronin S A and Cada M 2008 *Acta Mater.* **56** 696
[32] Gahan D, Dolinaj B and Hopkins M B 2008 *Plasma Sources Sci. Technol.* **17** 035026
[33] Hayden C, Gahan D and Hopkins M B 2009 *Plasma Sources Sci. Technol.* **18** 025018
[34] Child C D 1911 *Phys. Rev.* (*Ser. 1*) **32** 492
[35] Langmuir I 1913 *Phys. Rev.* **2** 450
[36] Kawamura E, Vahedi V, Lieberman M A and Birdsall C K 1999 *Plasma Sources Sci. Technol.* **8** R45
[37] Miller P A and Riley M E 1997 *J. Appl. Phys.* **82** 3689
[38] Godyak V A, Piejak R B and Alexandrovich B M 1992 *Plasma Sources Sci. Technol.* **1** 36
[39] Boswell R W, Lichtenberg A J and Vender D 1992 *IEEE Trans. Plasma Sci.* **20** 2
[40] Moseler M, Gumbsch P, Casiraghi C, Ferrari A C and Robertson J 2005 *Science* **309** 1545
[41] Pei Y T, Shaha K P, Chen C Q, Van der Hulst R, Turkin A A, Vainshtein D I and De Hosson J Th M 2009 *Acta Mater.* **57** 5156